

Design and Validation of Reconfigurable Foot for Bipedal Locomotion

Qixian Wang, Idris Wibowo, Vaibhav Malhotra, Ian Wong, Kelin Yu,
Seth Hutchinson, *Fellow, IEEE*, and Ye Zhao, *Senior Member, IEEE*

Abstract—Bipedal robots are garnering increasing interest due to their capability to operate across all terrains. A key factor affecting their mobility in varied terrains such as sandy or grassy landscapes is the foot’s ability to provide sufficient friction to minimize slipping and sinking. In this paper, we introduce an adaptive and reconfigurable foot design. Inspired by biological structures, the Tarsal segments and Cleats are included to augment the stability of bipedal robot locomotion. Additionally, a low-level torque controller has been designed to actuate the tarsals, working in concert with a high-precision terrain recognition algorithm that leverages multiple sensors. This allows the foot to alter its shape or the magnitude of applied torque in response to terrain characteristics. The adaptive reconfigurable foot has undergone extensive testing and has been successfully implemented on the Cassie robot, demonstrating its efficacy in enhancing robot mobility on complex terrains, particularly on soft surfaces like sand.

Index Terms—Mechanism design; Legged robot; Torque control.

I. INTRODUCTION

BIPEDAL robots possess characteristics such as high stability, agility, and load-carrying capabilities, making them suitable for a variety of tasks carried out on different terrains. They boast capabilities to carry out complex tasks in uncharacterized or dangerous environments. Notable examples include Cassie and Digit, which have achieved success in demanding scenarios such as cargo handling on uneven surfaces [1] and exploration of uncharacterized terrains [2]. While the design of motion planning and control algorithms plays an important role in the ability of a bipedal locomotion system to adapt to dramatic shifts in terrain conditions and instantaneous changes in ground contact mechanics, the range of conditions over which dynamic stability can be achieved are also heavily influenced by the morphological and mechanical configurations of the [3]. Traditionally, the legged robotics community has focused on designing and controlling robots via proximally actuated joints, which is amenable for locomotion purposes on hard surfaces, reducing the control complexity of the robot. However, the proximally actuated robots are limited in their gaits design, which assumes that the foot does not slide during contact. This assumption does not hold on loosely consolidated surfaces where the contacting limbs can easily slide due to unpredictable terrain deformation. Therefore, the adaptive robotic feet could provide a promising solution to promote robotic performance on deformable slopes [4].

Many teams have conducted research on adaptive foot design of legged robots, such as optimizing joint configurations

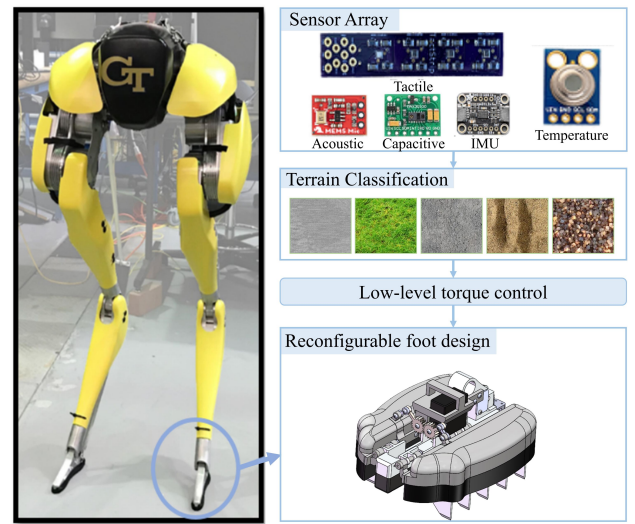


Fig. 1. The study is centered on the development of a bipedal foot mechanism. Sensor data are collected and employed within a terrain classification algorithm. This algorithm’s output subsequently informs the low-level torque controller’s response. The tarsal segments will be actuated according to terrain property.

and actuation systems, and they have achieved considerable progress [5] [6]. However, these studies primarily focus on quadruped robots, and comprehensive research on the feet of bipedal robots is still lacking. These researches, on the other hand, is illustrative to biped design for they verified the importance of contact area and contact stability. The lack of contact stability results in traditional slender bipedal feet’s being prone to sliding and sinking issues, especially in loose or uneven terrains [7]. Compared to quadruped robots, bipedal robots are usually heavier, have a higher center of gravity, and have comparatively smaller contact area when in locomotion. All these factors combined means more friction is needed for bipedal robot to reduce slippery. Current adaptive foot design for quadrupedal robots are mostly passive [8], which unsuitable for bipedal robot for not producing enough traction force. As a result, more analysis on the ways to minimize slippery is imperative [9], and one possible solution will be reconfigurable foot with actuators.

Furthermore, the physical properties of different terrains vary significantly [10]. For example, walking on cement versus grass will places different demands on the robot’s feet, and walking on rough stone road versus mud means the foot should have different configurations. While some passive feet have commendable performance on certain terrains [11], they

cannot dynamically adjust their feet configurations based on terrain requirements, making it difficult to meet the demands of all-terrain operations [12]. Reconfiguration robot, however, can be adjusted to fit rough terrains, therefore increasing the contact area and friction. As a result, more reconfigurable bipedal foot designs which can reduce bipedal robot slippery and enable robots to walk on different types of terrain is necessary.

In this paper, a bio-inspired reconfigurable foot design is introduced. To enhance stability during motion on uneven terrain and address the issue of foot sinking, two motor-driven tarsal segments are added. A lower-level impedance controller is applied to control the motors, altering the foot configuration. Passive cleats are also designed on the tarsal segments to further increase friction on soft ground. Additionally, pressure sensors are placed at the bottom of the foot and utilized for terrain recognition and contact sensing.

II. RELATED WORKS

In this section, the previous works on adaptive foot design, sensor allocation, and terrain classification algorithms will be introduced.

Adaptive foot design: The principles underlying the development of adaptive foot designs often find their source of inspiration in bipedal creatures [13] or quadrupeds [6] [14] renowned for their adeptness at traversing challenging terrains. A notable exemplar in this regard is the mountain goat, celebrated for its remarkable prowess in scaling nearly perpendicular cliffs [15].

The distinct tarsal segments present in the mountain goat's anatomy afford it augmented contact surfaces and enhanced frictional capabilities [16], however, the tarsal segments in previous work is not tested. In this paper, comprehensive experiments will be conducted to verify its functionality.

Tactile sensor: Sensorized Foot for Enhanced Environmental Awareness: In the pursuit of equipping legged robots with an understanding of their working environments, sensorized feet have been developed and experimented. Diverse components, including force/torque sensors [17] [18] [19], cameras [20], audio sensors [21], and inertial measurement units (IMU) [4], have been integrated into the feet of legged robots, catering to various functional requirements.

Recently, tactile sensors are broadly used in robotic sensing [22] [23]. However, it is noteworthy that conventional sensors are frequently characterized by high costs and low robustness. In this study, we present a self-fabricated, miniaturized, high-precision sensors [24] will be incorporated into the robotic foot, effecting a substantial reduction in cost while fortifying endurance.

Terrain classification: Owing to the diversity of operational environments of bipedal robots, the acquisition of terrain-related information is important. Machine learning and neural networks for terrain classification has been extensively explored [25] [26].

While previous researches have yielded impressive accuracy in terrain classification [16] [27], the direct integration of terrain data into the design of bipedal feet has remained relatively

unexplored. Therefore, this study introduces a novel concept of reconfigurable foot design. Based on the outcomes of terrain classification, this design enables dynamic adjustments to foot configurations, thus facilitating adaptability to varying terrains.

III. DESIGN

An adaptive reconfigurable robotic foot has been developed, targeting at the objective of minimizing slippage during bipedal robot locomotion. Motor actuated tarsal segments which allow modulation of the ground contact mechanics for the bipedal robot are designed and evaluated. To facilitate precise and rapid modulation, a low-level torque control scheme has been implemented, ensuring accurate actuation of the tarsal segments.

To enhance the robot's locomotion information, the sole of the foot has been equipped with two high-precision tactile sensors. These sensors provide data for terrain classification algorithm, enabling the bipedal robot to adapt to varying environmental conditions with improved stability and efficiency.

A. Mechanical Structure

The structure of the reconfigurable foot in shown in Fig. 2. Fig.2a illustrates the assembly of the foot mechanism. The motor is attached to the central foot via a bracket. The motor's placement, facilitated by the bracket, ensures the intersection of the two gear segments along the foot's central axis. A pair of tarsal segments are placed on each side of the foot, providing enhanced lateral rotational flexibility. Fig.2b details the layout of a single tarsal segment. The two tarsals, interconnected with gears, move synchronously.

1) Foot soles: The foot sole is composed of 60-hardness heat-resistant silicone, a material slightly softer than that used in the original design, enhancing the robot's ability to traverse rough terrains without sacrificing stability. The rubber pad, with a thickness of 20 mm, demonstrates minimal compression under stress; tests indicate that with a 30 kg force applied, it compresses only about 2 mm. The sole area of each tarsal segment is 6891 mm², and the central part is 1935 mm². To increase friction, the rubber surface features striped indentations, each 2 mm wide and deep. Furthermore, as depicted in Fig. 2c, two barometric tactile sensors and a capacitive sensor are embedded within the rubber pad for enhanced functionality.

2) Tarsal segments: The tarsal segments are constructed from PLA plastic to minimize weight. These segments are connected to the central part through a specially designed linkage, enhancing both durability and ease of replacement in case of damage. After experimental investigation, each tarsal is outfitted with five cleats, each being 30 mm wide, capable of penetrating the ground to a maximum depth of 35 mm. Detailed results of experiments are presented in Section V. The cleats on the two tarsals feature a triangular notch, oriented differently to avoid contact with the ground during lifting. To prevent breakage of the tarsals, two measures are implemented: 1) The cleats are fabricated from aluminum for increased strength; 2) Each cleat is passively actuated by a

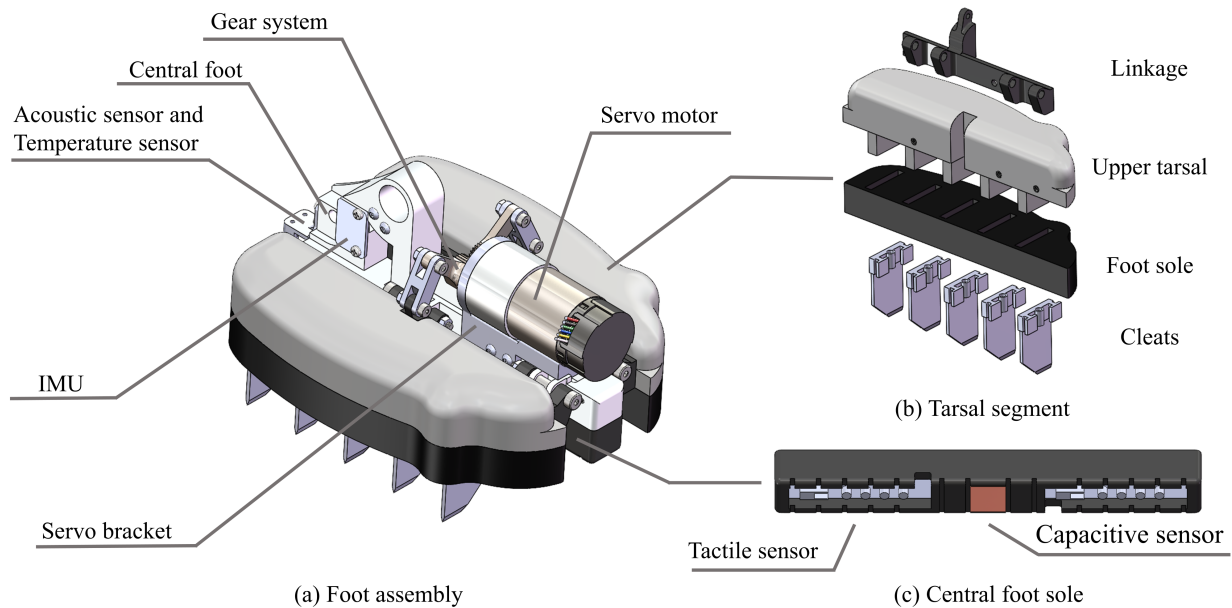


Fig. 2. Overview of the bipedal foot mechanism: (a) displays the entire structural layout; (b) highlights the tarsal segments, each outfitted with five cleats. The central foot section houses three sensors, complemented by tactile and capacitive sensors embedded within the sole (c).

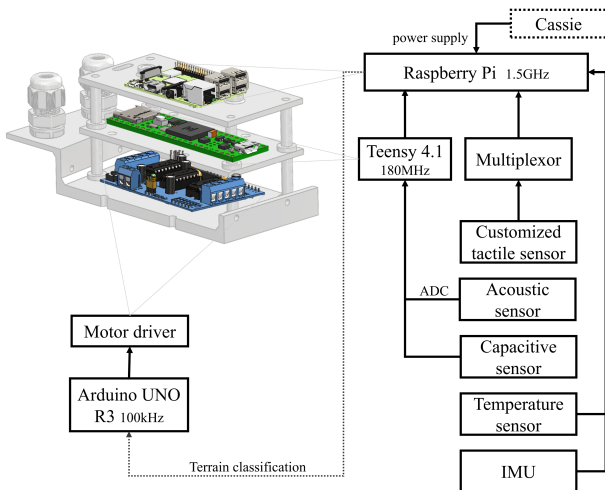
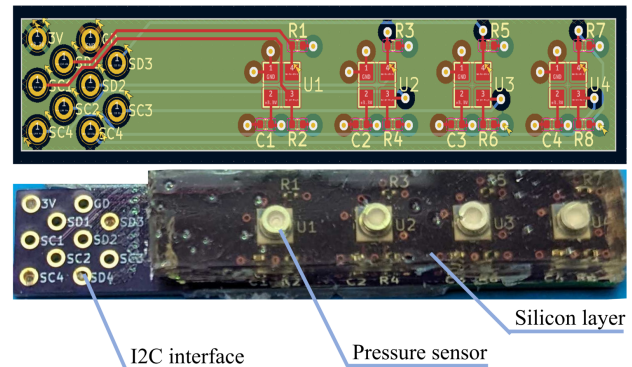


Fig. 3. Overview of the bipedal foot mechanism: (a) displays the entire structural layout; (b) highlights the tarsal segments, each outfitted with five cleats. The central foot section houses three sensors, complemented by tactile and capacitive sensors embedded within the sole (c).

spring with a stiffness of 0.14 lb/mm, allowing them to retract under excessive force.

The tarsal segments exhibit a maximum swing range from -26.6° to $+45^\circ$, which is sufficient for the intended application. It is also worth noting that one side of the cleats has been cut into a triangle. When the robot moves on hard surfaces and the tarsals are fully retracted, This design prevents the extended cleats from contacting the ground.

3) Motor and gear system: A brushed DC motor (37Dx70L, Pololu metal gear-motor) is utilized to actuate the tarsal segments. Operating at a voltage of 24V, this servo is capable of producing a maximum torque of 23 kg-cm, sufficient for fast actuation of both tarsal segments. The gear mechanism



comprises two customized cylindrical gears, which are 3D-printed out of high-stiffness materials. Additionally, rocker arms are connected to the gears. One gear is mounted directly on the motor, while the other is positioned on the motor bracket.

4) Wiring and enclosure: The extensive array of sensors in the design posed a significant challenge in wire management. To effectively address this, multi-core wires were selected, along with a redesign of the central foot to facilitate wire routing. An enclosure, specifically designed for housing all the electrical components, will be mounted atop the Cassie robot, as shown in Fig. 3.

To minimize the impact of the foot's mass on locomotion control, the design centered around low-mass construction. Consequently, the finalized foot has a mass of 1.15 kg. In comparison, Cassie's original foot is 0.25 kg.

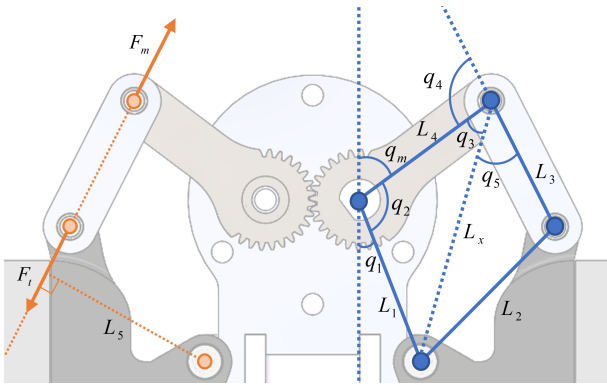


Fig. 5. Diagram of Mechanical Structure

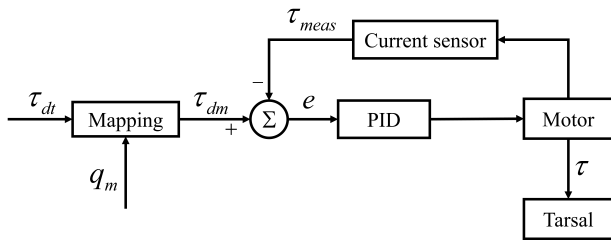


Fig. 6. Block diagram of low-level torque control

B. Electronic Structure

The electronics of the foot are comprised of an inertial measurement unit (IMU) (MPU-6050), an acoustic sensor (Sparkfun SPH8878LR5H), a capacitive sensor, an infrared temperature sensor (HiLetgo GY-906 MLX90614ESF), two customized tactile barometric sensor arrays, two microcontroller boards (Teensy 3.6 and Arduino UNO R3), a motor driver (Texas Instruments L293D) and a single board computer (Raspberry Pi 4 Model B), as shown in Fig. 3.

The tactile sensor array is a custom 4-layer PCB each containing four barometric sensors (Measurement Specialties MS583730BA01-50 MEMS). To receive viable force readings from the barometric sensors, 20A hardness silicone is cast directly onto the PCB. To manage the data from the eight identical barometric sensors, a TCA9548A multiplexer is employed.

The IMU, tactile sensors, temperature sensor, and Teensy all communicate as slaves via a single 100 kHz inter-integrated circuit (I²C) bus to the Raspberry Pi. Because all eight barometric sensors on the two tactile sensors have the same hardware address, four separate I²C buses must travel from each tactile sensor to the I²C multiplexer to be consolidated onto a single bus. The capacitive strip is soldered directly to a Teensy pin containing hardware capacitive sensing at the speed of 180 MHz. The acoustic sensor outputs a single analog signal to the Teensy as the Raspberry Pi lacks analog-to-digital converters (ADCs). After some data processing and feature extraction from capacitive and acoustic data, key information is sent along the I²C bus to the Raspberry Pi. The terrain classification described in [16] is executed on the Raspberry Pi, with the outcomes subsequently transmitted to an Arduino to control the motor's operation.

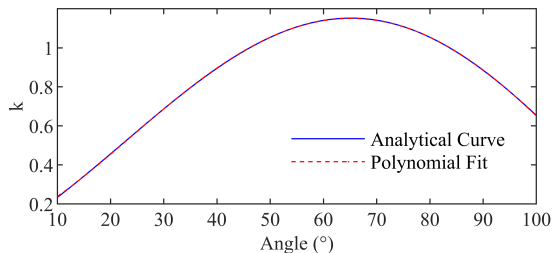


Fig. 7. The curve obtained from mathematical calculations (blue) and the fitted curve (red) are shown in the figure, with their discrepancies falling within an acceptable range.

IV. IMPLEMENTATION

A. Dynamic modeling and Low-Level Torque Control

The most effective method to evaluate the control efficacy of the system involves measuring the torque and angle of the tarsal segment. However, since the parameters directly controllable are those of the servo, constructing a dynamic model of the system is crucial for achieving accurate control. A simplified structural diagram illustrating this is presented in Fig. 5, where q_m represents the servo angle, a parameter that can be measured by the angular encoder of the motor, $L_1 - L_4$ the length of links and L_5 the force arm.

Given the mechanical structure of the linkage system, it is obvious that:

$$L_x = (L_1^2 + L_4^2 - 2 \cos q_2 L_1 L_4)^{\frac{1}{2}} \quad (1)$$

where $q_2 = \pi - q_1 - q_m$. Then:

$$\theta_2 = \arccos\left(\frac{L_x^2 + L_3^2 - L_2^2}{2 L_x L_3}\right) \quad (2)$$

Then θ_1 can be calculated. Subsequently, the force exerted on the rocker arm can be expressed as follows:

$$F_m = \frac{\tau}{L_4 \sin \theta_1} \quad (3)$$

where τ is the output torque of the motor. Since $F_t = F_m$, the torque applied to the tarsal can be described as:

$$\tau_t = F_t L_x \sin \theta_2 \quad (4)$$

Based on the mathematical relation above, a Low-level torque control is constructed to enable the tarsal segment track desired torque. This will prevent the servo from overheat, while imply enough force to create traction. Fig. 6 indicates the block diagram of the proposed controller. Due to the fact that the control objective is τ_t while τ is the parameter that can be controller directly, a dynamic mapping is adopted to convert the desired torque of the tarsal τ_{dt} to the desired torque of the motor τ_{dm} . According to Eq.3 and Eq.4, the relation can be demonstrated as:

$$k\tau = \tau_t, k = \frac{L_x \sin \theta_2}{L_4 \sin \theta_1} \quad (5)$$

The trend of k as a function of q_m is shown in Fig. 7. For ease of mathematical computation, we employ polynomial fitting to approximate the curve. Table 1 displays the

TABLE I
RSME FOR DIFFERENT POLYNOMIAL ORDERS

Order	5	4	3	2
RSME	2.5×10^{-4}	1.1×10^{-3}	1.1×10^{-2}	0.03

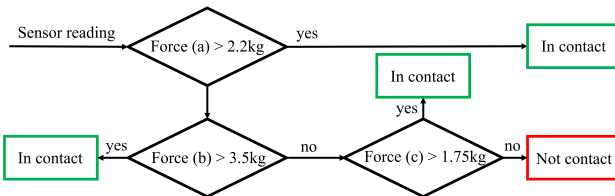


Fig. 8. Illustration of the Contact Detection Algorithm: 'Force (a)' represents the average data from all eight tactile sensors, 'Force (b)' denotes the average data within a single sensor array, and 'Force (c)' signifies the maximum data recorded by an individual tactile sensor.

RSME (Root Mean Square Error) for polynomials of varying complexities. Due to the high accuracy and low computational complexity, a quartic polynomial is selected.

In normal operation, Cassie takes one step every 0.5 second. To increase the actuation speed, the parameters of PID controller are set to be large.

B. Force Sensing and Contact Detection

Within the central segment's rubber pad, a pair of tactile sensor arrays are integrated at a separation of 9 mm. The newly designed tactile sensor array comprises four small barometric sensors arranged uniformly in a row, with a spacing of 114 mm. Consequently, this configuration yields a total of eight force detection points.

The design ensures data acquisition even when the contact area is constrained, such as in terrains with rough stones where only one or two small barometric sensors might establish contact. This capability maintains the validity of collection of force measurements, enabling reliable contact detection under varying contact conditions.

Contact detection is necessary for the operation of the reconfigurable foot. Enabling it to retract the tarsals upon elevation and actuate the tarsals upon ground contact. To facilitate this, data from tactile sensors is employed. The multi-layer detector is demonstrated in Fig. 8.

The threshold values are established with consideration to the tactile sensor area (120mm^2), the central segment area (3084mm^2), and Cassie's weight (35 kg). Additionally, tests were conducted to measure the stepping force of the Cassie robot on a force plate, yielding an average force of 300 N and a maximum force of 450 N. The detector's primary objective is to ascertain precise contact detection when the robot's foot interacts with varying terrains. For instance, during locomotion over gravel when only a subset of sensors is activated, if the reading from any single sensor surpasses the designated threshold, contact is confirmed.

C. Terrain Classification

In our prior research [16], [27], we augmented the original Cassie foot with an combination of sensors—temperature,

acoustic, inertial measurement unit (IMU), capacitive, and tactile. Utilizing the data harvested from these sensors, we designed and validated a terrain classification algorithm. This high accuracy terrain classification algorithm is adaptable to an array of terrain conditions. Our classification approach leverages Random Forests as the foundational classifier, enhanced by a memory function to account for temporal dependencies, thereby bolstering classification efficacy.

The selection of terrains aimed at simulating both indoor and outdoor terrain environments, including wood boards, foam mats, gravel, concrete blocks, and poppy seeds, among others. The collected sensor data were processed using a feature-based classification algorithm that combines Random Forests with a custom-designed memory function. Cross-validation outcomes affirm the algorithm's robustness, with a classification accuracy as high as 96.3%.

In this work, we deploy the aforementioned classification algorithm to inform the adaptive configuration of the robot's foot mechanism. Specifically, the actuation of the tarsal segments is modulated based on the classification results to optimize interaction with various terrains. On rigid and level surfaces such as concrete and metal, the tarsal segments remains inactive to prevent potential damage to the substrate and the foot's cleats. Conversely, when traversing solid, irregular terrain like large stones, the tarsals engage with small torque to safeguard the cleats whilst ensuring sufficient grip. In scenarios involving pliable terrains such as sand and poppy seeds, which demand augmented traction for stable locomotion, the tarsal segments are actuated at higher desired torques to mitigate slippage.

This terrain-responsive strategy enables the robot to adapt its locomotion dynamically, optimizing stability and interaction with diverse environmental conditions.

D. System Architecture

V. RESULTS AND DISCUSSION

A. Test Setup

To evaluate the functionality of the reconfigurable foot, a series of tests were conducted: individual functional test, ground contact test, and robot test.

During the individual functional tests, both the control efficacy and force sensing accuracy were scrutinized. The gear system is interfaced with a () servo motor. To facilitate position feedback, the servo motor is modified to include an additional signal feedback wire. Position tracking precision is examined with the foot anchored to a test stand under a no-load condition, with the objective of assessing the upper limits of actuation speed and confirming that the proposed foot design supports standard locomotion patterns. Force sensing precision is verified by applying force to the foot against a calibrated scale. Given the unique contact dynamics of bipedal locomotion, the normal force is measurement by the tactile sensor, exclusively.

In the ground contact tests, the performance of the reconfigurable foot is compared against the standard Cassie foot in both friction coefficient and sinking depth. An Instron testing machine (model number), capable of exerting a consistent force, is employed for these evaluations. Traction force is

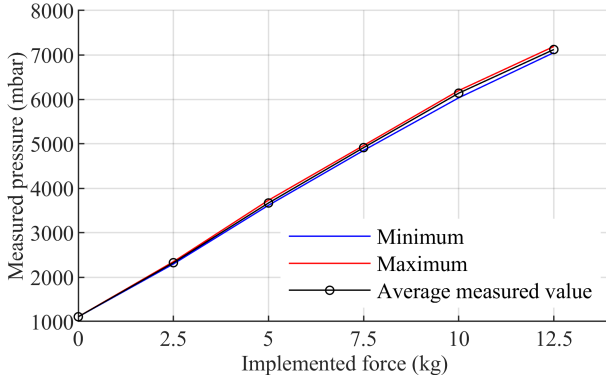


Fig. 9. Data Collection for Force: 20 measurements were obtained for each applied force, with the maximum, minimum, and average values depicted for each set.

quantified using a force gauge. In an effort to simulate commonly encountered terrains and granular media, the tests were conducted on a carefully selected array of surfaces, including (shown in figure ()):

- Grass: artificial turf with an approximate thickness of 2 cm.
- Carpet: wool carpet, approximately 5 mm thick.
- Gravel: consisting of crushed stones with diameters ranging from 2 to 6 mm.
- Sawdust: a mixture of sawdust and paper scraps with diameters ranging from 1 mm to 1 cm.
- Sand: For ease of experimentation, poppy seeds with an approximate diameter of 1 mm are used to simulate sand.

In robot tests, the foot is fixed on Cassie robot. Using the data gathered from IMU, we are able to calculate the slippery distance of Cassie. Experiments were performed on three different terrains, sand, grass and concrete. To clearly quantify the slippery distance, slippery metrics is utilized and can be defined as follows:

where the denominator is the distance travelled by the robot body, and the numerator indicates the travel distance of the reconfigurable foot when it is in contact with the ground.

B. Individual Functional Test Result

The tactile sensor's precision is critical for both terrain classification and contact detection accuracy. During experimentation, varying forces were administered centrally to a sensor array using a force gauge. The correlation between the sensor data (the mean value obtained from the four tactile sensors) and the applied force is depicted in Fig. 9. The results suggest that the sensor's linearity, when subjected to forces of up to 15 kg, is within acceptable limits and meets the requirements for terrain classification. And the characterization function can be expressed as:

$$F_s = 488N + 1161.6 \quad (6)$$

where F_s is the reading of the sensor, N is the value of applied force.

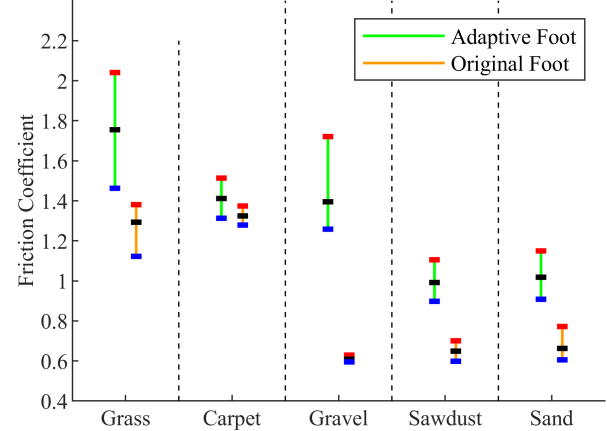


Fig. 10. Comparison of Friction Coefficient Between Adaptive Reconfigurable Foot and Original Cassie Foot.

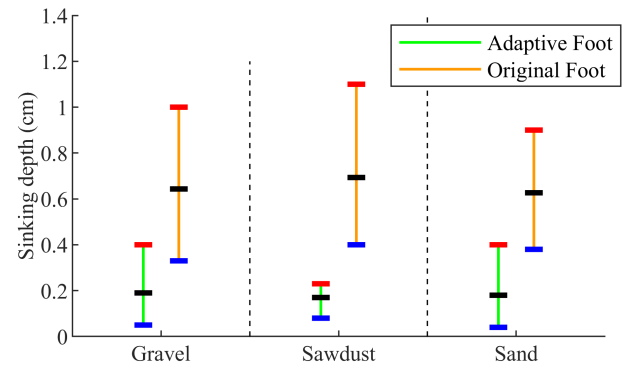


Fig. 11. Comparison of Sinking Depth Between Adaptive Reconfigurable Foot and Original Cassie Foot.

C. Ground Contact Test Result

In the ground contact tests, we evaluated the friction coefficient and sinking depth for both the adaptive reconfigurable foot and the original Cassie foot.

For the friction coefficient test, a 3 kg metal block was affixed to each foot, with tarsal segments actively actuated throughout the testing process. Results, as depicted in Fig. 10, reveal that, except on the carpet, the new foot demonstrates significantly enhanced friction performance on various terrains compared to the original foot. On grass, the cleats play a pivotal role, deeply embedding into the terrain to generate substantial resistance. It is a feature absent in original Cassie foot. Given that artificial grass is plastic and has a higher friction coefficient with rubber than natural grass, the adaptive foot's advantages are further pronounced on natural grassy terrains. On gravel, the increase in friction is most notable, as the cleats embed into the gravel, offering additional resistance. In softer terrains like sawdust and sand, both the cleats and tarsal segments contribute to increased friction. However, on carpet, where cleats cannot penetrate, the improvement in friction is less obvious. In the sinking depth test, the foot was positioned on the terrain, and a 3 kg metal block was dropped

onto the foot from a height of 10 cm. We measured the foot's positions before and after the impact, as illustrated in Fig. 11. The results show a notable reduction in sinking depth across three terrains, attributable to the larger contact area of the new foot design.

These findings suggest that the adaptive reconfigurable foot not only significantly enhances friction, thereby reducing slippage, but also prevents the robot from sinking into various terrains. This demonstrates its considerable potential for improving bipedal locomotion performance.

D. Robot Test Result

VI. CONCLUSION

ACKNOWLEDGMENTS

REFERENCES

- [1] A. Shamsah, Z. Gu, J. Warnke, S. Hutchinson, and Y. Zhao, "Integrated task and motion planning for safe legged navigation in partially observable environments," *IEEE Transactions on Robotics*, pp. 1–22, 2023.
- [2] J.-K. Huang and J. W. Grizzle, "Efficient anytime clif reactive planning system for a bipedal robot on undulating terrain," *IEEE Transactions on Robotics*, vol. 39, no. 3, pp. 2093–2110, 2023.
- [3] C. Semini, V. Barasuol, J. Goldsmith, M. Frigerio, M. Focchi, Y. Gao, and D. G. Caldwell, "Design of the hydraulically actuated, torque-controlled quadruped robot hyq2max," *IEEE/ASME Transactions on Mechatronics*, vol. 22, no. 2, pp. 635–646, 2017.
- [4] G. Valsecchi, R. Grandia, and M. Hutter, "Quadrupedal locomotion on uneven terrain with sensorized feet," *IEEE Robotics and Automation Letters*, vol. 5, no. 2, pp. 1548–1555, 2020.
- [5] R. Käslin, H. Kolvenbach, L. Paez, K. Lika, and M. Hutter, "Towards a passive adaptive planar foot with ground orientation and contact force sensing for legged robots," in *2018 IEEE/RSJ International Conference on Intelligent Robots and Systems (IROS)*, 2018, pp. 2707–2714.
- [6] M. G. Catalano, M. J. Pollayil, G. Grioli, G. Valsecchi, H. Kolvenbach, M. Hutter, A. Bicchi, and M. Garabini, "Adaptive feet for quadrupedal walkers," *IEEE Transactions on Robotics*, vol. 38, no. 1, pp. 302–316, 2022.
- [7] A. Chatterjee, A. Mo, B. Kiss, E. C. Gönen, and A. Badri-Spröwitz, "Multi-segmented adaptive feet for versatile legged locomotion in natural terrain," in *2023 IEEE International Conference on Robotics and Automation (ICRA)*, 2023, pp. 1162–1169.
- [8] D. Liu, M. Sun, and D. Qian, "Structural design and gait simulation of bionic quadruped robot," in *2018 International Conference on Advanced Mechatronic Systems (ICAMechS)*, 2018, pp. 16–20.
- [9] M. Yamada, H. Maie, Y. Maeno, S. Sano, and N. Uchiyama, "Design of point-contact type foot with springs for biped robot," in *2010 IEEE/ASME International Conference on Advanced Intelligent Mechatronics*, 2010, pp. 806–811.
- [10] A. Karsai, D. Kerimoglu, D. Soto, S. Ha, T. Zhang, and D. I. Goldman, "Real-time remodeling of granular terrain for robot locomotion," *Advanced Intelligent Systems*, vol. 4, no. 12, p. 2200119, 2022. [Online]. Available: <https://onlinelibrary.wiley.com/doi/abs/10.1002/aisys.202200119>
- [11] H. Kolvenbach, P. Arm, E. Hampp, A. Dietsche, V. T. Bickel, B. Sun, C. Meyer, and M. Hutter, "Traversing steep and granular martian analog slopes with a dynamic quadrupedal robot," *CoRR*, vol. abs/2106.01974, 2021. [Online]. Available: <https://arxiv.org/abs/2106.01974>
- [12] C. Yao, G. Shi, Y. Ge, Z. Zhu, and Z. Jia, "Predict the physics-informed terrain properties over deformable soils using sensorized foot for quadruped robots," in *2023 International Conference on Advanced Robotics and Mechatronics (ICARM)*, 2023, pp. 330–335.
- [13] K. Enomoto, T.-Y. Chen, T. Kawasetsu, and K. Hosoda, "Design of a robotic foot with midtarsal joint locking mechanism," in *2022 IEEE 5th International Conference on Soft Robotics (RoboSoft)*, 2022, pp. 1–6.
- [14] S.-A. Abad, N. Sornkarn, and T. Nanayakkara, "The role of morphological computation of the goat hoof in slip reduction," in *2016 IEEE/RSJ International Conference on Intelligent Robots and Systems (IROS)*, 2016, pp. 5599–5605.
- [15] M. Lindong, S. Bo, X. Peng, L. Zhenjie, J. Chenxing, D. Ruina, and D. Qindan, "A strategy to climb vertical cliffs for the quadruped robot imitating goat," in *2018 3rd International Conference on Control, Robotics and Cybernetics (CRC)*, 2018, pp. 37–41.
- [16] T. Tyler, V. Malhotra, A. Montague, Z. Zhao, F. L. H. I. au2, and Y. Zhao, "Integrating reconfigurable foot design, multi-modal contact sensing, and terrain classification for bipedal locomotion," 2023.
- [17] H. Kolvenbach, C. Bärtschi, L. Wellhausen, R. Grandia, and M. Hutter, "Haptic inspection of planetary soils with legged robots," *IEEE Robotics and Automation Letters*, vol. 4, no. 2, pp. 1626–1632, 2019.
- [18] M. Wang, M. Wonsick, X. Long, and T. Padre, "In-situ terrain classification and estimation for nasa's humanoid robot valkyrie," in *2020 IEEE/ASME International Conference on Advanced Intelligent Mechatronics (AIM)*, 2020, pp. 765–770.
- [19] W. Bosworth, J. Whitney, S. Kim, and N. Hogan, "Robot locomotion on hard and soft ground: Measuring stability and ground properties in-situ," in *2016 IEEE International Conference on Robotics and Automation (ICRA)*, 2016, pp. 3582–3589.
- [20] Y. N. Khan, A. Masselli, and A. Zell, "Visual terrain classification by flying robots," in *2012 IEEE International Conference on Robotics and Automation*, 2012, pp. 498–503.
- [21] A. Kurobe, Y. Nakajima, K. Kitani, and H. Saito, "Audio-visual self-supervised terrain type recognition for ground mobile platforms," *IEEE Access*, vol. 9, pp. 29970–29979, 2021.
- [22] Y. Han, K. Yu, R. Batra, N. Boyd, C. Mehta, T. Zhao, Y. She, S. Hutchinson, and Y. Zhao, "Learning generalizable vision-tactile robotic grasping strategy for deformable objects via transformer," 2023.
- [23] K. Yu, Y. Han, M. Zhu, and Y. Zhao, "Mimictouch: Learning human's control strategy with multi-modal tactile feedback," 2023.
- [24] T. De Clercq, A. Sianov, and G. Crevecoeur, "A soft barometric tactile sensor to simultaneously localize contact and estimate normal force with validation to detect slip in a robotic gripper," *IEEE Robotics and Automation Letters*, vol. 7, no. 4, pp. 11767–11774, 2022.
- [25] F. Vulpi, A. Milella, R. Marani, and G. Reina, "Recurrent and convolutional neural networks for deep terrain classification by autonomous robots," *Journal of Terramechanics*, vol. 96, pp. 119–131, 2021. [Online]. Available: <https://www.sciencedirect.com/science/article/pii/S0022489820301117>
- [26] M. M. Venâncio, R. S. Gonçalves, and R. A. d. C. Bianchi, "Terrain identification for humanoid robots applying convolutional neural networks," *IEEE/ASME Transactions on Mechatronics*, vol. 26, no. 3, pp. 1433–1444, 2021.
- [27] X. Guo, B. Blaise, J. Molnar, J. Coholich, S. Padte, Y. Zhao, and F. L. Hammond, "Soft foot sensor design and terrain classification for dynamic legged locomotion," in *2020 3rd IEEE International Conference on Soft Robotics (RoboSoft)*, 2020, pp. 550–557.